Inorganic Chemistry

Article

pubs.acs.org/IC

Isoquinoline-Based Lanthanide Complexes: Bright NIR Optical Probes and Efficient MRI Agents

Fabien Caillé,[†,‡] Célia S. Bonnet,[†] Frédéric Buron,[‡] Sandrine Villette,[†] Lothar Helm,[§] Stéphane Petoud,*[,†] Franck Suzenet,*[,‡] and Éva Tóth*[,†]

[†]Centre de Biophysique Moléculaire, UPR 4301 CNRS, rue Charles Sadron, 45071 Orléans, France

[‡]Institut de Chimie Organique et Analytique, UMR 7311 CNRS/Université d'Orléans, rue de Chartres, 45067 Orléans, France

[§]Laboratory of Inorganic and Bioinorganic Chemistry, Ecole Polytechnique Fédérale de Lausanne, BCH, 1015 Lausanne, Switzerland

Supporting Information

ABSTRACT: In the objective of developing ligands that simultaneously satisfy the requirements for MRI contrast agents and near-infrared emitting optical probes that are suitable for imaging, three isoquinoline-based polyaminocarboxylate ligands, **L1**, **L2** and **L3**, have been synthesized and the corresponding Gd^{3+}, Nd^{3+} and Yb^{3+} complexes investigated. The specific challenge of the present work was to create NIR emitting agents which (i) have excitation wavelengths compatible with biological applications and (ii) are able to emit a sufficient number of photons to ensure sensitive NIR detection for microscopic imaging. Here we report the first observation of a NIR signal arising from a Ln^{3+} complex in aqueous solution in a microscopy setup. The lanthanide complexes have high thermodynamic stability (log K_{LnL} =17.7−18.7) and good selectivity for lanthanide ions versus the endogenous cations Zn^{2+}, Cu^{2+}, and Ca^{2+} thus preventing transmetalation. A variable temperature and pressure ^{17}O NMR study combined with nuclear magnetic relaxation dispersion measurements yielded the microscopic parameters characterizing water exchange and rotation. Bishydration of the lanthanide cation in the complexes, an important advantage to obtain high relaxivity for the Gd^{3+} chelates, has been demonstrated by ^{17}O chemical shifts for the Gd^{3+} complexes and by luminescence lifetime measurements for the Yb^{3+} analogues. The water exchange on the three Gd^{3+} complexes is considerably faster (k_{ex}^{298} = (13.9−15.4) × 10^6 s^{-1}) than on commercial Gd^{3+}-based contrast agents and proceeds *via* a dissociative mechanism, as evidenced by the large positive activation volumes for Gd**L1** and Gd**L2** (+10.3 ± 0.9 and +10.6 ± 0.9 cm^3 mol^{-1}, respectively). The relaxivity of Gd**L1** is doubled at 40 MHz and 298 K in fetal bovine serum (r_1 = 16.1 vs 8.5 mM^{-1} s^{-1} in HEPES buffer), due to hydrophobic interactions between the chelate and serum proteins. The isoquinoline core allows for the optimization of the optical properties of the luminescent lanthanide complexes in comparison to the pyridinic analogues and provides significant shifts of the excitation energies toward lower values which therefore become more adapted for biological applications. **L2** and **L3** bear two methoxy substituents on the aromatic core in ortho and para positions, respectively, that further modulate their electronic structure. The Nd^{3+} and Yb^{3+} complexes of the ligand **L3**, which incorporates the *p*-dimethoxyisoquinoline moiety, can be excited up to 420 nm. This wavelength is shifted over 100 nm toward lower energy in comparison to the pyridine-based analogue. The luminescence quantum yields of the Nd^{3+} (0.013−0.016%) and Yb^{3+} chelates (0.028−0.040%) are in the range of the best nonhydrated complexes, despite the presence of two inner sphere water molecules. More importantly, the 980 nm NIR emission band of Yb**L3** was detected with a good sensitivity in a proof of concept microscopy experiment at a concentration of 10 μM in fetal bovine serum. Our results demonstrate that even bishydrated NIR lanthanide complexes can emit a sufficient number of photons to ensure sensitive detection in practical applications. In particular, these ligands containing an aromatic core with coordinating pyridine nitrogen can be easily modified to tune the optical properties of the NIR luminescent lanthanide complexes while retaining good complex stability and MRI characteristics for the Gd^{3+} analogues. They constitute a highly versatile platform for the development of bimodal MR and optical imaging probes based on a simple mixture of Gd^{3+} and Yb^{3+}/Nd^{3+} complexes using an identical chelator. Given the presence of two inner sphere water molecules, important for MRI applications of the corresponding Gd^{3+} analogues, this result is particularly exciting and opens wide perspectives not only for NIR imaging based on Ln^{3+} ions but also for the design of combined NIR optical and MRI probes.

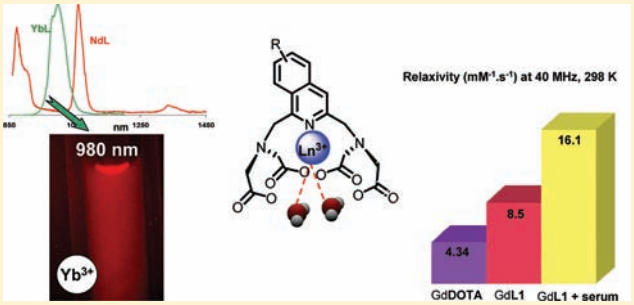

Received: November 14, 2011
Published: January 10, 2012

1. INTRODUCTION

In the last two decades, lanthanide coordination chemistry has witnessed a spectacular evolution, largely promoted by the successful use of lanthanide complexes in biomedical applications. Millions of clinical magnetic resonance imaging (MRI) examinations are carried out after the injection of Gd^{3+} chelates.[1] Luminescent lanthanide complexes are also gaining more and more importance for *in vitro* optical assays and cellular optical imaging.[2,3] Although these applications often use similar ligand structures for the formation of stable lanthanide complexes, mainly poly(aminocarboxylates), they all have their specific requirements with respect to the ligand design and there has been relatively little interaction between these different research fields. Recently, bimodal or multimodal imaging has emerged as a novel concept to ascertain observations made in one imaging modality by a complementary technique. Each of the state-of-the-art imaging modalities has its own advantages and weaknesses, and the assessment of a biological problem often requires the use of more than one imaging approaches, applied either successively or, in an ideal case, simultaneously. MRI provides morphological images of an excellent spatial and temporal resolution; however, it suffers from low sensitivity. Nuclear imaging techniques such as SPECT or PET have several orders of magnitude better sensitivity than MRI, but their resolution is inherently limited. The advantages of optical imaging are its relatively low cost, small instruments and excellent detection sensitivity, however, in limited resolution at the macroscopic level. Like nuclear imaging, optical techniques cannot produce anatomical images. Therefore coupling MRI to nuclear or optical techniques is of major interest for multimodal imaging.

Ideally, bimodal imaging is performed by using bimodal probes that combine the characteristics required for both imaging modalities within a single molecular entity. Such bimodal probes ensure identical biodistribution observed in the different imaging modalities, resulting in easier interpretation and merging of the images. A simplified chemical design, characterization and formulation of the imaging probe is another benefit. In MRI-optical bimodal imaging, previous work has been mostly done with nanoparticles containing Gd^{3+} complexes and organic dyes which allowed validating *in vivo* MRI experiments based on colocalization of the acquired MR and optical images.[4,5]

Our major interest is to use lanthanide chelates as bimodal imaging agents for combined MRI and optical detection. Given the diverse magnetic and optical properties of lanthanide ions, lanthanide complexes are perfectly suited for the design of MRI and optical bimodal probes. Its high electron spin (7/2) and slow electronic relaxation make Gd^{3+} the most efficient paramagnetic cation for MRI contrast agent applications.[6] On the other hand, several lanthanides have visible and/or near-infrared emission, with unique advantages over organic fluorescent probes and luminescent semiconductor nanocrystals, including high resistance to photobleaching, temporal discrimination through long luminescence lifetimes, absence of reabsorption effects and spectral discrimination due to their narrow emission bands.[2,3,7] The simplest design of a bimodal MRI-optical agent involves the development of ligand systems that simultaneously satisfy the requirements for the two imaging modalities, and a simple mixture (in the concentration ratio dictated by the sensitivity limit of each modality) of the paramagnetic Gd^{3+} complex and the luminescent lanthanide complex, both formed with the same ligand, could be used as bimodal imaging probe. It can be particularly advantageous to apply a single chelator for the Gd^{3+} and the luminescent lanthanide ion, instead of using two different ligands, in macromolecular agents such as dendrimers, for instance.

The structural requirements for the complexes to be used in MRI and in luminescence have been considered for a long time irreconcilable. While the presence of inner sphere water molecule(s) in a Gd^{3+} chelate is an absolute condition for its MRI efficiency, the presence of water close to a lanthanide cation is considered as detrimental for the luminescence properties due to the quenching generated by the O−H oscillator. We have recently demonstrated that the presence of even two H_2O bound to the Ln^{3+} is not an absolute limitation for the development of near-infrared (NIR) luminescent probes.[8] Indeed, the Nd^{3+} complexes of the pyridine-based ligand **Py** and its derivative were shown to have remarkable luminescence intensity in the NIR, despite the presence of two inner sphere water molecules, highly beneficial for the MRI activity of the corresponding Gd^{3+} chelate. In addition, we have shown that the Nd^{3+} and Yb^{3+} complexes formed with these pyridine-based ligands and their triazole derivatives have interesting features for both MRI and luminescence applications.[9] The thermodynamic stability of the complexes is reasonably high, and their kinetic inertness is particularly high for a bishydrated chelate, thanks to the rigidification of the ligand skeleton by the pyridine ring. Indeed, the dissociation rate constant has been comparable to that for GdDTPA, a clinical contrast agent (H_5DTPA = diethylenetriaminepentaacetic acid). The nontoxicity of the complexes has been evidenced in a detailed *in vitro* and *in vivo* (in mice) toxicity study.[9] The two inner sphere water molecules in the Gd^{3+} complex undergo fast water exchange and are not replaced by endogenous anions. Finally, the pyridine is an efficient sensitizer of NIR luminescence of Nd^{3+} and Yb^{3+}. Their respective quantum yields obtained are comparable to the best, *nonhydrated* NIR emitting Ln^{3+} complexes reported in aqueous solution. From an optical point of view, the parent pyridine complexes have nevertheless excitation wavelengths corresponding to high energy (~260 nm), which are far from ideal for biological applications due to the interferences between the photons and biological material, leading to its perturbation and potential destruction. This excitation energy has been shifted toward lower energy of *ca.* 50 nm upon attachment of triazole derivative to the pyridine ring.[9] In an attempt to further optimize this parameter by shifting the excitation energy toward lower energy for biological applications while keeping intact the lanthanide chelating unit that provides favorable complexation and relaxation properties, we have synthesized a series of isoquinoline derivative ligands, **L1**, **L2** and **L3** (Chart 1). **L2** and **L3** possess electron donor substituents expected to further contribute to the decrease of the excitation energy. The acid−base properties of the ligands and the thermodynamic stability of their complexes formed with lanthanides and endogenous cations have been assessed by pH-potentiometry experiments. The relaxation properties of the Gd^{3+} complexes have been characterized in a combined variable temperature ^{17}O NMR and ^{1}H nuclear magnetic relaxation dispersion (NMRD) studies. The water exchange mechanism has been determined from variable pressure ^{17}O NMR measurements. Finally, we have performed photophysical characterization of the near-infrared emitting complexes formed with Yb^{3+} and Nd^{3+}. We have tested an Yb^{3+} emitting complex in an imaging experiment demonstrating that these molecules can be potentially used as NIR optical imaging agents under practical conditions.

dx.doi.org/10.1021/ic202446e | *Inorg. Chem.* 2012, 51, 2522−2532

Chart 1. Isoquinoline and Pyridine-Based Ligands for Ln^{3+} Complexation

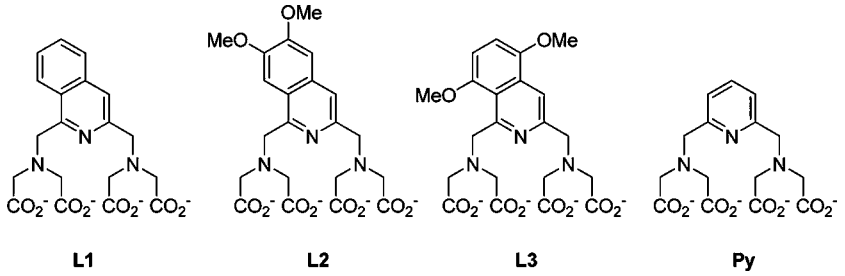

2. RESULTS AND DISCUSSION

2.1. Syntheses of the Isoquinoline Ligands. The synthesis of the isoquinoline derivative **L1** was achieved from commercially available benzaldehyde (Scheme 1). Improvements

Scheme 1. Synthesis of Ligand L1[a]

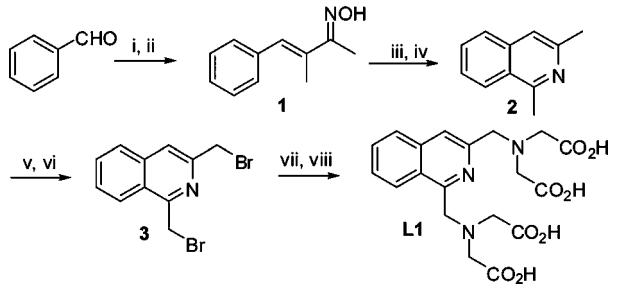

[a](i) 2-Butanone, $HCl_{(g)}$, rt, 90%; (ii) NH_2OH, toluene, reflux, 92%; (iii) PCl_5, decalin, 0 °C then P_2O_5, decalin, 180 °C, 60%; (iv) NBS, benzoyl peroxide, CCl_4, reflux; (v) $HPO(OEt)_2$, DIEA, THF, rt, 35% over two steps; (vi) $HN(CH_2CO_2Et)_2$, K_2CO_3, KI, CH_3CN, reflux; (vii) LiOH, THF/H_2O (1/1), rt 89% over two steps.

of the procedure described by Zielinski were realized to yield the key intermediate isoquinoline **2**.[10] Aldol condensation between benzaldehyde and 2-butanone afforded the α,β-unsatured ketone which reacted with hydroxylamine to yield the oxime **1**. Beckmann rearrangement followed by Bischler–Napieralski cyclization afforded the isoquinoline **2** in good yield. Inspired by the work from Yin and Tan,[11] bromination of the two methyls was realized using *N*-bromosuccinimide (NBS) followed by additional treatment with diethyl phosphite and diisopropylethylamine (DIEA) to give 1,3-dibromomethyl-isoquinoline **4**. Nucleophilic substitution with diethyl iminodiacetate and subsequent saponification afforded ligand **L1** in almost quantitative yield after purification on ion-exchange resin.

Substituted ligands **L2** and **L3** were synthesized following a different approach reported elsewhere.[12]

2.2. Thermodynamic Studies. *2.2.1. Protonation Constants.* The protonation constants, log K_{Hi}, of the three ligands **L1**, **L2** and **L3**, as defined in eq 1, were determined by pH-potentiometric titrations at I = 0.1 M KCl, 298 K.

$$K_{Hi} = \frac{[H_iL]}{[H_{i-1}L][H^+]} \quad (1)$$

Four protonation constants could be determined for each ligand. The titration curves are presented in Figure 1 and S1 in the Supporting Information, and the calculated protonation constants are shown in Table 1. The first two protonation

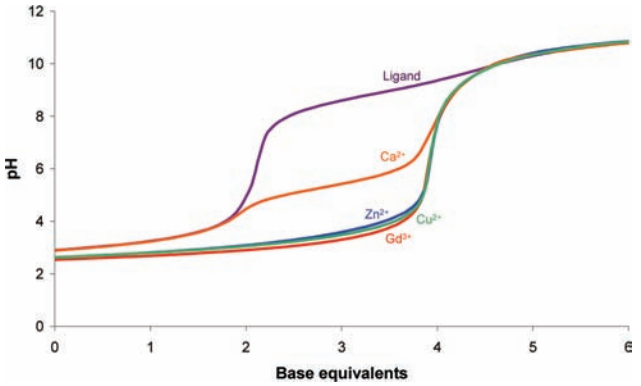

Figure 1. Potentiometric titration curves of aqueous solutions containing 1.11 mM **L1** with 0 or 1 equiv of $CaCl_2$, $ZnSO_4$, $CuCl_2$ or $GdCl_3$. I = 0.1 M KCl; 298 K.

Table 1. Protonation Constants of the Three Ligands Measured in KCl (0.1 M) at 298 K

log K_{Hi}	L1	L2	L3	Py[b]
log K_{H1}	8.83(7)[a]	8.84(7)	9.39(2)	8.95
log K_{H2}	8.55(5)	8.44(5)	8.53(2)	7.85
log K_{H3}	3.04(3)	3.02(9)	3.04(3)	3.38
log K_{H4}	2.54(5)	2.56(6)	2.54(3)	2.48
$\sum$(log K)	22.96	22.86	23.50	22.66

[a]The error indicated in the parentheses corresponds to two times the standard deviation. [b]From ref 8.

constants correspond to the protonation of the amine nitrogens while the third and fourth constants represent the protonation of the carboxylic functions. The protonation of the isoquinoline nitrogen is never observed, as in the case of **Py** and its derivatives,[8,9] as well as analogous ligands containing only one iminodiacetate arm or two iminodiacetate arms directly linked to the pyridine,[13] and other ligands containing a pyridine moiety.[14,15] The replacement of the pyridine scaffold by an isoquinoline does not lead to a significant change in the overall basicity of the ligand ($\sum$(log K_{HL1}) = 22.96; $\sum$(log K_{HLpy}) = 22.66) despite an increase in the total electronic density. This increase is expected to mostly affect the nitrogen of the isoquinoline, whose protonation is not observed, and which is far away from the other protonation sites to significantly influence them. The only difference between the pyridine and the isoquinoline derivatives is observed in log K_{H2}. The introduction of methoxy groups on the isoquinoline have negligible effect on the acid–base properties of the ligands, and indeed the protonation constants of **L1**, **L2**, and **L3** are very similar except for log K_{H1} of **L3**, which is slightly higher. This could be explained by the proximity between the amine nitrogen

dx.doi.org/10.1021/ic202446e | Inorg. Chem. 2012, 51, 2522–2532

concerned and one of the methoxy groups which could stabilize the protonated form of the nitrogen given its electron-donating capacities.

2.2.2. Stability Constants of the Complexes. Complex stability constants, log K_{ML}, and complex protonation constants, log K_{HML} (eqs 2 and 3), have been determined for complexes formed with various lanthanide ions (Ln^{3+}) and endogenous cations such as Zn^{2+}, Ca^{2+} and Cu^{2+} by direct potentiometric titrations (KCl 0.1 M, 298 K) in a typical pH-range 1.9−3.5.

$$K_{ML} = \frac{[ML]}{[M][L]} \quad (2)$$

$$K_{HML} = \frac{[HML]}{[H][ML]} \quad (3)$$

The titration curves for 1/1 ligand/metal ratios are shown in Figure 1 and Figures S2−S4 in the Supporting Information, and the stability constants of the complexes are presented in Table 2.

Table 2. Stability Constants and Selectivity Constants of the Different Complexes Measured by Potentiometric Titration in KCl (0.1 M) at 298 K

log K	L1	L2	L3	Py[b]	EDTA[c]
log K_{NdL}	18.60(8)[a]	18.65(6)	17.73(3)	18.76	16.51
log K_{EuL}	18.45(7)			18.90	17.25
log K_{GdL}	18.2(1)	18.94(9)	18.53(4)	18.60	17.35
log K_{LuL}	18.10(8)	19.21(9)	17.76(3)		19.74
log K_{CaL}	9.54(9)	9.75(4)	9.56(5)	9.43	10.65
log K_{CuL}	16.43(8)	16.0(2)	16.90(7)	15.69	18.78
log K_{HCuL}	3.54(9)	4.25(7)	3.73(6)	3.45	3.1
log K_{ZnL}	16.13(9)	15.48(7)	15.78(3)	15.84	16.5
log K_{HZnL}	3.82(5)	4.15(2)	3.77(2)	3.81	3.0
log K_{sel}[d]	6.35	7.09	6.68	7.07	4.2

[a]The error indicated in parentheses corresponds to two times the standard deviation. [b]From ref 8 except for log K_{EuL}. [c]From ref 13. [d]$K_{sel} = K_{therm}(\alpha_H^{-1} + \alpha_{Ca}^{-1} + \alpha_{Zn}^{-1} + \alpha_{Cu}^{-1})^{-1}$ with $\alpha_H^{-1} = 1 + K_{H1}[H^+] + K_{H1}K_{H2}[H^+]^2 + ...$; $\alpha_{Ca}^{-1} = K_{CaL}[Ca^{2+}]$; $\alpha_{Zn}^{-1} = K_{ZnL}[Zn^{2+}]$; $\alpha_{Cu}^{-1} = K_{CuL}[Cu^{2+}]$; calculated for $[Ca^{2+}]$ = 2.5 mM, $[Zn^{2+}]$ = 50 μM, $[Cu^{2+}]$ = 1 μM at pH 7.4.

The stability constants of the Ln^{3+} complexes with the various ligands fall in the range log K_{ML} = 17.7−19.2. When compared to EDTA (H_4EDTA = ethylenediaminetetraacetic acid), the introduction of the pyridine ring increases the overall basicity of the ligand ($\sum$(log K_{HEDTA}) = 20.9; $\sum$(log K_{HL}) > 22.6) making them better complexing agents, especially for the early lanthanide ions. When looking at the stability constants in more details, one can draw several conclusions: (i) no trend can be detected along the lanthanide series; (ii) the behavior of the three ligands toward Ln^{3+} ions is very similar, and the stability constants are very close to those obtained for the parent compound **Py**. This latter result was expected as there was no difference in the basicity of the ligands and the complexing unit remains the same for **Py** and the isoquinoline derivatives. The introduction of the methoxy moieties on the isoquinoline scaffold does not have a critical influence on the basicity and consequently on the coordinating properties of the ligands. Nevertheless, it should be noted that, despite its highest basicity, **L3** displays slightly less stable complexes with Ln^{3+} than **L1** or **L2**, which can probably be explained by steric effects as the methoxy groups are closer to the coordination site when they are in *para* position.

The stability constants formed with Gd^{3+} and the various ligands are all in the range 18.2−18.9. The toxicity of MRI contrast agents is highly correlated to the release of free Gd^{3+}, and it has been demonstrated that the thermodynamic stability is not sufficient to assess the toxicity of the complexes.[16] The selectivity of the ligand for Gd^{3+} over endogenous cations and, more importantly, the kinetic inertness of the Gd^{3+} complex[17] are key factors for its *in vivo* toxicity. We investigated the thermodynamics of complexation of endogenous cations (Zn^{2+}, Cu^{2+}, and Ca^{2+}) in order to determine the selectivity of the ligands. In the case of Cu^{2+} and Zn^{2+}, the experimental data could be satisfactorily fitted with the introduction of a monoprotonated complex; all stability constants are reported in Table 2. The selectivity for lanthanide ions over Zn^{2+}, Cu^{2+}, and Ca^{2+} is conserved for the isoquinoline derivatives. The selectivity constants, K_{sel}, defined by Cacheris et al.,[16] which take into account the competition of those endogenous cations, are comparable to that for DTPA (log $K_{selDTPA}$ = 7.0), and higher than K_{sel} of EDTA (Table 2. The kinetic inertness, as demonstrated for Gd**Py**, is remarkable for this family of bishydrated chelates and can be attributed to the rigid aromatic skeleton and to the absence of dinuclear Zn^{2+} complexes that are an important driving force in the transmetalation of Gd**DTPA**.[8] No dinuclear complexes are detected with **L1**, **L2**, and **L3**, either. In addition, the *in vivo* nontoxicity of Ln**Py** complexes has also been demonstrated previously.[9]

2.3. Relaxation Characteristics of the Gd Complexes. In order to characterize the parameters governing the proton relaxivity of complexes Gd**L1**, Gd**L2**, and Gd**L3**, we have performed a variable temperature and variable pressure ^{17}O NMR study combined with proton relaxation rate measurements at different magnetic fields and temperatures. Transverse ^{17}O relaxation rates and chemical shifts were measured as a function of the temperature on aqueous solutions of Gd**L1**, Gd**L2**, Gd**L3**, and on a diamagnetic reference solution ($HClO_4$, pH 4) at 11.7 T. The nuclear magnetic relaxation dispersion profiles were measured between 10 kHz and 80 MHz at 298 K, 310 K, and 323 K.

For all three Gd^{3+} complexes, we considered two inner sphere water molecules (q = 2), as determined by luminescent lifetimes measurements of Yb^{3+} complexes in H_2O and D_2O (see below). Bishydration was confirmed by the experimental ^{17}O chemical shifts (which are proportional to the Gd^{3+} concentration and to q).

The experimental data were analyzed with the Solomon−Bloembergen−Morgan (SBM) theory to yield the microscopic parameters of the complexes characterizing water exchange and rotation (see the Supporting Information for equations). As Figure 2 and Figures S5 and S6 in the Supporting Information show, the ^{17}O reduced transverse relaxation rates ($1/T_{2r}$) first slightly increase (up to ca. 290 K) and then decrease with increasing temperature, indicating that the complexes are mainly in the intermediate and fast exchange region. Here $1/T_{2r}$ is defined by the transverse relaxation rate of the bound water oxygen, $1/T_{2m}$, which is in turn influenced by the water exchange rate, k_{ex}, the longitudinal electronic relaxation rate, $1/T_{1e}$, and the scalar coupling constant, $A/\hbar$. The reduced ^{17}O chemical shifts are determined by $A/\hbar$. The transverse ^{17}O relaxation is governed by the scalar relaxation mechanism and thus contains no information on the rotational motion of the system. If we are not interested in detailed information about the electron spin relaxation and if we restrict the analysis of the

dx.doi.org/10.1021/ic202446e | Inorg. Chem. 2012, 51, 2522−2532

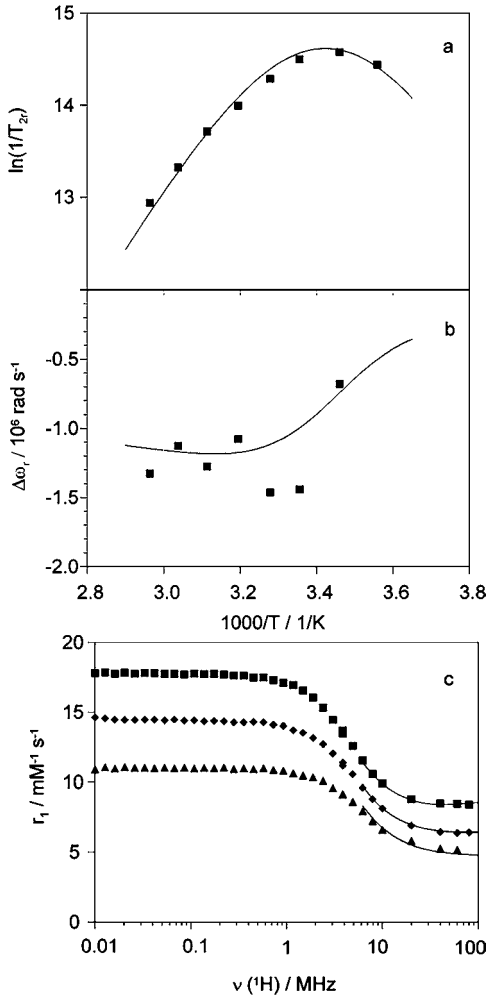

Figure 2. Temperature dependence of the reduced ^{17}O (a) transverse relaxation rates, (b) chemical shifts of Gd**L1** at 11.7 T. (c) NMRD profiles of Gd**L1** at 25 °C (■), 37 °C (◆), and 50 °C (▲). The curves represent the simultaneous fit to the experimental data points.

NMRD data to medium and high magnetic fields, the SBM approach gives reliable information on dynamic processes like water exchange and rotational correlation times for small complexes.[18,19] Therefore we included only relaxivity values above 6 MHz in the simultaneous fit and the following parameters have been thus adjusted: the water exchange rate, k_{ex}^{298}, the activation enthalpy for water exchange, $\Delta H^{\ddagger}$, the scalar coupling constant, $A/\hbar$, the rotational correlation time, τ_R^{298}, and its activation energy, E_R, and the parameters describing electron spin relaxation, the mean square of the zero field splitting, Δ^2, the correlation time for the modulation of the zero field splitting, τ_V^{298}, while its activation energy, E_V, has been fixed to 1 kJ/mol. A small empirical constant describing the outer sphere contribution to the ^{17}O chemical shift, C_{os}, was also fitted to account for the lower values of chemical shifts obtained for Gd**L2** and Gd**L3**. The diffusion coefficient D_{GdH}^{298} and its activation energy E_{DGdH} were fixed to 26×10^{-10} m^2 s^{-1} and 22 kJ mol^{-1}, respectively. The Gd−water proton distance was fixed to r_{GdH} = 3.1 Å, and the closest approach between the Gd^{3+} ion and the outer sphere protons to a_{GdH} = 3.6 Å. The parameters resulting from the best fit are presented in Table 3.

The water exchange rates are four times higher than the one of Gd**DTPA**. This is consistent with the general observation that bishydrated complexes have faster exchange than monohydrated complexes.[21,22] The exchange rates are very similar for the three isoquinoline-based complexes, and ∼50% higher than that on Gd**Py**, its methoxy and triazole derivatives.[8,9] Similarly to the pyridine derivatives, the aromatic system in the isoquinoline chelators rigidifies the ligand skeleton and has a slight accelerating effect on the water exchange. The substitution by methoxy groups does not affect the coordination sphere of the metal ion and consequently has only little influence on the water exchange rate.

As expected, the rotational correlation times are longer compared to the Gd**DTPA** complex due to the higher molecular weight of the complexes. The methoxy-substituted isoquinolines have a significantly higher rotational correlation time due to their larger size and more hydrophilic nature, compared to the unsubstituted isoquinoline.

In order to assess the mechanism of the water exchange, we have performed variable pressure ^{17}O NMR studies which give access to the activation volume, $\Delta V^{\ddagger}$.[6] $\Delta V^{\ddagger}$, defined as the difference between the partial molar volume of the transition state and the reactants, allows assigning the mechanism of the water exchange as it is assumed to be a direct measure of the degree of bond changes (making, breaking, lengthening) occurring in the transition state. $\Delta V^{\ddagger}$ is related to the pressure dependence of the exchange rate constant through eq 4:

$$\frac{1}{\tau_m} = k_{ex} = (k_{ex})_0^T \exp\left\{ -\frac{\Delta V^{\ddagger}}{RT} P \right\} \quad (4)$$

where $(k_{ex})_0^T$ is the water exchange rate at zero pressure and temperature T. Transverse ^{17}O relaxation rates, $1/T_{2r}$, were

Table 3. Parameters Obtained from the Fitting of the Transversal ^{17}O NMR Relaxation Rates as a Function of Temperature and Pressure, of the Chemical shifts as a Function of Temperature at 11.7 T, and of the NMRD Profiles at 298 K, 310 K, and 323 K

	Gd**L1**	Gd**L2**	Gd**L3**	Gd**Py**[a]	Gd**DTPA**[b]
k_{ex}^{298} ($10^6 s^{-1}$)	13.9(7)	15.4(8)	14.1(6)	9.3	3.3
$\Delta H^{\ddagger}$ (kJ mol^{-1})	52.5(8)	42.2(6)	41.0(6)	50.5	51.6
$\Delta S^{\ddagger}$ (J mol^{-1} K^{-1})	+69(2)	+38(3)	+16(1)	+ 57.6	+ 53.0
$\Delta V^{\ddagger}$ (cm^3 mol^{-1})	+10.3(9)	+10.6(9)		+ 8.8	+12.5
τ_R^{298} (ps)[a,b]	112(4)	173(5)	160(5)	91.5	58
E_R (kJ mol^{-1})	19.9(2)	22.9(2)	19.6(2)	20.2	17.3
τ_v^{298} (ps)[c]	3.1(1)	2.0(1)	2.2(1)	2.8	25
Δ^2 ($10^{20} s^{-1}$)	0.50(5)	0.56(3)	0.64(6)	0.96	0.46
$A/\hbar$ (10^6rad s^{-1})	−3.8(1)	−3.8(1)	−3.8(1)	−3.7	−3.8
C_{os}	0.0	0.10(5)	0.20(5)	0.0	0.18

[a]From ref 9. [b]From ref 20.

dx.doi.org/10.1021/ic202446e | Inorg. Chem. 2012, 51, 2522−2532

measured at 9.4 T and two different temperatures, 298 and 343 K, for Gd**L1** and Gd**L2**. No significant changes in the relaxation rates were observed with pressure at 298 K (see Figure S7 in the Supporting Information) since the contribution of the water exchange to $1/T_{2r}$ is small at this temperature (k_{ex} represents ~20% in the correlation time, $1/\tau_{s1} = k_{ex} + 1/T_{1e}$, see the Supporting Information). Therefore no pressure effect is observable on the measured T_2 values. At 343 K, the systems are in the fast exchange regime where the transverse relaxation rates are proportional to $1/k_{ex}$. The increase of $1/T_{2r}$ with pressure is thus due to the slowing down of the water exchange process, suggesting a dissociatively activated exchange. $A/\hbar$ has been previously found independent of pressure for different lanthanide(III) aqua ions.[23] As nothing is known about the pressure dependence of the electronic relaxation, in the analysis of the variable pressure ^{17}O NMR data we have checked that a reasonable pressure variation of τ_v ($|\Delta V_v^{\ddagger}| \leq 4$ cm^3 mol^{-1}) had no significant effect on the calculated activation volume. The experimental variable pressure ^{17}O relaxation data together with the best fits are presented Figure 3 and Figure S8 in the

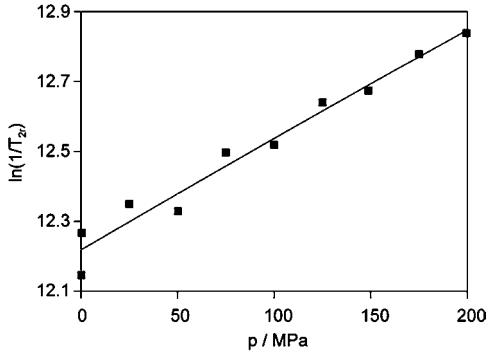

Figure 3. Pressure dependence of reduced ^{17}O transverse relaxation rates of Gd**L1** at 9.4 T and 70 °C. The curve represents the simultaneous fit to the experimental data points.

Supporting Information, and the resulting activation volumes are reported in Table 3. $(k_{ex})_0^T$ was calculated to be 3.5×10^8 s^{-1} and 2.8×10^8 s^{-1} for Gd**L1** and Gd**L2**, respectively. The activation volumes have high positive values, typical of a dissociatively activated water exchange, in agreement with the positive activation entropies. Only few data have been reported concerning the mechanism of water exchange on bishydrated Gd^{3+} complexes. Those with an overall coordination number of 8 had associative water exchange.[24−26] The activation volumes for those isoquinoline-based complexes are slightly higher than that for Gd**Py** and its triazole derivative, Gd**C5TPy**,[9] but still lower than $\Delta V^{\ddagger}$ of Gd**DTPA**, which has an almost limiting dissociative mechanism.[27]

We have also measured the NMRD profile of Gd**L1** in 100% fetal bovine serum (FBS) and compared to the profile obtained in 4-(2-hydroxyethyl)-1-piperazineethanesulfonic acid (HEPES) buffer (Figure S9 in the Supporting Information). Given the hydrophobic nature of the isoquinoline moiety, noncovalent binding is expected between the complex and serum albumin through hydrophobic interactions. The NMRD curve displays the typical "hump" of slow rotating complexes between 10 and 80 MHz (at 40 MHz, 298 K, the relaxivity is nearly doubled in FBS compared to HEPES buffer) confirming that the complex is bound to proteins of the serum through hydrophobic interactions.

2.4. Absorption and NIR Luminescence Properties of the Complexes. The UV−vis absorption spectra of the different lanthanide complexes were measured in HEPES buffer at room temperature and are presented in Figure 4 for the Yb^{3+}

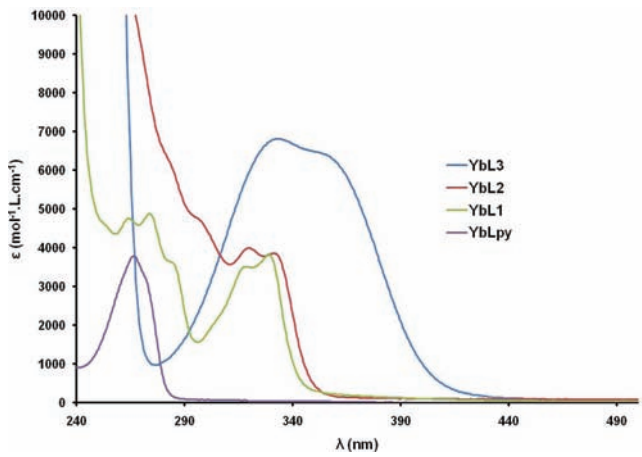

Figure 4. UV−vis absorption spectra of the Yb^{3+} complexes (1 mM) in 0.01 M HEPES, pH 7.0.

complexes and S14 (Supporting Information) for the Nd^{3+} complexes. Upon coordination, the $\pi-\pi^*$ transition bands centered on the ligands in all complexes experience a red shift of *ca.* 5−10 nm (see Figures S10−S12 in the Supporting Information). This change is accompanied by a strong decrease of the molar absorptivity for **L3** and to a lesser extent for **L2**, and by a small increase for **L1**. These effects can be attributed to the perturbation of the electronic structure of the ligand upon lanthanide coordination, making this transition more allowed compared to the free ligand when the isoquinoline is not substituted, and less allowed when the methoxy groups are present. Considering the maximum of the electronic envelope, a red shift of the $\pi-\pi^*$ transition band of almost 100 nm was obtained for both Yb^{3+} and Nd^{3+} complexes by replacement of the pyridine ring with an isoquinoline sensitizing moiety, and by further addition of methoxy groups. The substitution at C5 and C8 positions (**L3**) gives a higher red shift as compared to substitution at C6 and C7 positions. Excitation on these bands in all six complexes resulted in the observation of NIR emission spectra that contains the typical sharp emission bands corresponding to the specific emission of Nd^{3+} or Yb^{3+}. Nd^{3+} and Yb^{3+} complexes formed with **L1**, **L2**, and **L3** display metal-centered NIR luminescence in aqueous solution, at pH 7 and at room temperature upon excitation at 320 nm, 335 nm, and 360 nm respectively. Emission, excitation and UV−Vis spectra of the Nd**L3** and Yb**L3** complexes are displayed in Figure 5. The corresponding spectra for **L1**, and **L2** complexes are shown in Figures S18 and S19 in the Supporting Information. The Yb^{3+} complexes display a NIR emission band ranging from 920 to 1050 nm, which is assigned to the $^2F_{5/2} \rightarrow {}^2F_{7/2}$ transition. For the Nd^{3+} complexes, individual apparent maxima of emission bands were observed at 873, 1059, and 1328 nm and are attributed to the transitions arising from the $^4F_{3/2}$ level to the $^4I_{9/2}$, $^4I_{11/2}$ and $^4I_{13/2}$ sublevels respectively.

The presence of these luminescence bands clearly shows that isoquinoline-based scaffolds are capable of sensitizing these excited states efficiently, which was further confirmed by recording the excitation spectra of the Yb^{3+} and Nd^{3+}

dx.doi.org/10.1021/ic202446e | *Inorg. Chem.* 2012, 51, 2522−2532

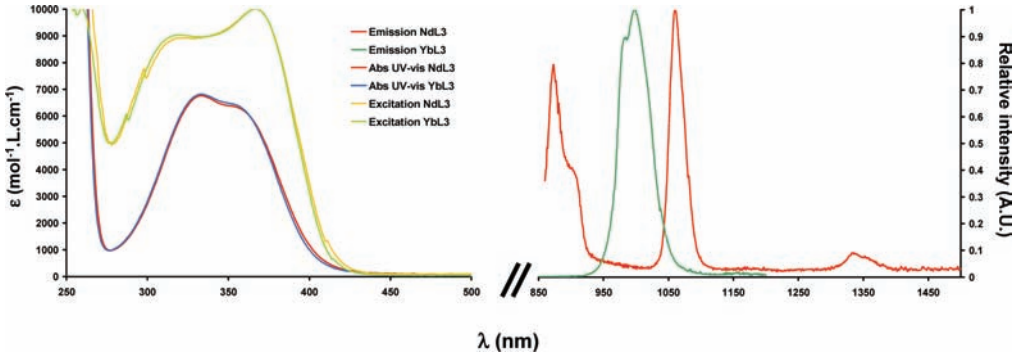

Figure 5. Absorption, normalized emission (λ_{ex} = 360 nm) and excitation (λ_{em} = 1053, and 980 nm respectively) spectra of 1 mM of Nd**L3** and Yb**L3** in HEPES 0.01 M at pH 7.0.

complexes (fixing the emission at 980 nm, and 1054 nm respectively) (see Figure 5 and Figures S18 and S19 in the Supporting Information).

A similar shift of the band wavelength is observed on the excitation spectra of the complexes (Figures S15−S16 in the Supporting Information) upon monitoring the Nd^{3+}- or the Yb^{3+}-centered emission. A red shift of ca. 50 nm is detected between the apparent maxima of excitation bands of Ln**L1** and Ln**L3**. The **L3** ligand appears as the most promising sensitizer of the series for biological applications as excitation at low energies is important to minimize biological interactions and potential damage to biological media. Also, the higher the value of the excitation wavelength, the less autofluorescence resulting from biological media will be present for improved signal-to-noise ratio and detection sensitivity. **L3** can be excited at an energy as low as 420 nm (using the right side of the band located at the lowest energy), which is a shift of more than 100 nm with respect to the **Py** sensitizer.[9]

In order to analyze the photophysical processes occurring for these complexes, the energies of the singlet and triplet states of the ligand bound to lanthanide metal ions have been assessed. We have recorded the steady-state fluorescence and time-resolved phosphorescence spectra from the ligand bound to Gd^{3+} in the different complexes. Indeed, the Gd^{3+} electronic levels are too high in energy to allow ligand to lanthanide energy transfer. The fluorescence spectra obtained at room temperature all resulted in the presence of a broad band that is assigned to the S_1-S_0 transition with apparent maxima ranging from 28600 cm^{-1} (350 nm) for **L1** to 19900 cm^{-1} (505 nm) for **L3** (Table 4). Upon recording phosphorescence spectra with a delay of 0.1 ms after the excitation flash at low temperature (77 K), the band of the singlet state disappears, and a band corresponding to the triplet state appears. These bands have apparent maxima located at 19000 cm^{-1} (530 nm), 20200 cm^{-1} (495 nm), and 16800 cm^{-1} (594 nm) for **L1**, **L2**, and **L3** respectively (see Table 4 and Figure S17 in the Supporting Information). Even if these bands are more blue-shifted compared to the systems based on tropolonate[28] or on azulene ligands,[29] which have been both reported to sensitize NIR emitting lanthanide cations with a good efficiency,[29] there is a significant shift toward lower energies compared to the triplet state of **Py** which also sensitizes efficiently Nd^{3+} and Yb^{3+} luminescence and has a maximum energy located at 25400 cm^{-1} (393 nm).[8] Overall, these different shifts indicate that changes induced on the electronic structures of these sensitizers result in significant changes of the position of both energies of singlet and triplet states. These shifts are more important than those previously observed upon substitution of the pyridine core.[9]

Luminescence lifetimes upon monitoring the emission of the lanthanide cations were recorded in order to analyze the protection of the lanthanide cations against nonradiative deactivation and allowed the quantification of the number of inner sphere water molecules. The analysis of the experimental luminescence decays obtained upon excitation of the different complexes at 266 nm in water and deuterated water revealed all the best fittings as single-exponential functions. The fitted lifetimes upon monitoring Nd($^4F_{3/2}$) and Yb($^2F_{5/2}$) bands are summarized in Table 5.

Table 4. Singlet and Triplet State Energies (cm^{-1}) Recorded in Aqueous Solutions for the Different Complexes (1 mM), pH 7.0 (HEPES)

	L1	L2	L3	Py[c]
λ_{exc} (nm)	320	335	360	268
singlet[a]	28600	26500	19900	27800
triplet[b]	19000	20200	16800	25400

[a]Steady state fluorescence spectra recorded at 298 K (1 mM). [b]Time-resolved phosphorescence spectra recorded at 77 K with 0.1 ms delay after flash. Apparent maxima of emission bands are used for the estimation of the energies of the electronic levels. [c]From ref 9.

Table 5. Luminescence Lifetimes (τ) of Yb^{3+} and Nd^{3+} Complexes Formed with L1, L2 and L3 (1 mM) at pH 7 (HEPES, 10 mM) in Water and D_2O Solution, Quantum Yields (ϕ) and Number of Water Molecules Directly Coordinated to the Metal Ion (q)

			τ (μs)[b]		
complex	λ_{exc} (nm)[a]	ϕ (%), H_2O	H_2O	D_2O	q
Yb**L1**	320	0.040(4)	0.44(3)	8.1(5)	2.2(3)
Nd**L1**	320	0.016(2)	0.065(2)	0.323(5)	*c*
Yb**L2**	335	0.028(3)	0.54(3)	9.2(5)	1.5(3)
Nd**L2**	335	0.013(2)	0.069(2)	0.381(3)	*c*
Yb**L3**	340	0.039(4)	0.43(2)	8.5(4)	2.0(3)
Nd**L3**	340	0.016(2)	0.064(2)	0.312(3)	*c*
Yb**Lpy**[d]	266	0.022	0.384	7.9	2.3
Nd**Lpy**[e]	267	0.0097	0.059	0.310	*c*
Eu**Lpy**[e]	266		403	1850	2.1

[a]Excitation wavelength used for quantum yield measurements. [b]Luminescence lifetime decays were obtained upon excitation at 266 nm. [c]q values obtained for Nd^{3+} complexes do not reflect the evidenced bishydration of the complexes and, therefore, are not reported (see text). [d]From ref 9. [e]From ref 8.

dx.doi.org/10.1021/ic202446e | Inorg. Chem. 2012, 51, 2522−2532

They are roughly twenty times longer in deuterated water for Yb^{3+} complexes, and five times longer for Nd^{3+} complexes. The Yb^{3+} lifetimes in H_2O are consistent with those measured for the pyridine-based complexes and their triazole derivatives.[9] Lifetimes are significantly shorter than those reported for monohydrated complexes, such as DTPA,[30] 0.58 and 10.4 μs for Nd^{3+} and Yb^{3+} respectively, and for the nonhydrated T2soxMe developed by Bünzli et al.,[31] 0.15 and 2.47 μs for Nd^{3+} and Yb^{3+}, respectively. They are in the same order of magnitude as the bishydrated thqN-SO_3 recently reported by Mazzanti et al.,[32] 0.052 and 0.329 μs for Nd^{3+} and Yb^{3+}, respectively. The number of water molecules bound to the metal ions in the various complexes can be determined by using eqs 5[33,34]and 6:[35]

$$q = A(\Delta k_{obs}) - C \text{ for } Nd^{3+} \quad (5)$$

$$q = A(\Delta k_{obs} - B) \text{ for } Yb^{3+} \quad (6)$$

where A = 130 ns for Nd^{3+} and 1 μs for Yb^{3+}, B = 0.2 μs^{-1}, and C = 0.4; Δk_{obs} is given in ns^{-1} and μs^{-1} for Nd^{3+} and Yb^{3+}, respectively, $k_{obs} = 1/\tau_{obs}$, and $\Delta k_{obs} = k_{obs}(H_2O) - k_{obs}(D_2O)$. By applying those equations to the results obtained for the Yb^{3+} complexes, we obtain q values around 2 within the experimental error, which confirms the presence of two water molecules coordinated to the lanthanide as it was evidenced previously for the Gd^{3+} analogues. It should be noted that the slightly smaller value obtained for Yb**L2** may account for the fact that the empirical equation for Yb^{3+} has been established on the basis of data mostly obtained from nonhydrated or monohydrated complexes. For the Nd^{3+} complexes, the values are surprisingly smaller and tend to point to a q value of 1, which does not match the values obtained for Yb^{3+}. Nd^{3+} is a larger cation than Yb^{3+}, which could only lead to a higher coordination number for Nd^{3+}. However, as the lifetimes of the complexes in water are very short, a small experimental error on this value can induce a dramatic effect on the q values. Since (i) the corresponding Yb^{3+} and Gd^{3+} complexes are bishydrated, (ii) the q value of the **Py** complex has also been calculated with the corresponding Eu^{3+} complex and found to be 2.1, and (iii) all the ligands have the same coordination sphere, we do not expect the Nd^{3+} complexes to be monohydrated.

To quantify the intramolecular ligand to metal ion energy transfer efficiency in the different lanthanide complexes, luminescence absolute quantum yields were measured upon ligand excitation in H_2O, at pH 7 and at room temperature. The results are summarized in Table 5. The quantum yields of the Nd^{3+} complexes fall in the range 0.013−0.016%, and those of the Yb^{3+} complexes in the range 0.028−0.040%. The quantum yields are for each case higher for the Yb^{3+} than for the Nd^{3+} complexes indicating that these chromophores sensitize more efficiently Yb^{3+}. These quantum yields are in the same range than those obtained for the parent pyridine complexes and their triazole derivatives.[8,9] They are remarkable for bishydrated complexes in aqueous solution in which the presence of proximate O−H oscillators often induces a large quenching effect due to the small energy gap in these NIR-emitting cations. The Nd^{3+} quantum yields are 2 orders of magnitude higher than, and the Yb^{3+} quantum yield of the same order of magnitude as, those of the recently published bishydrated hydroxyquinolinate complexes.[32,36] For the Nd^{3+} chelates, they are in the same order of magnitude as those of nonhydrated complexes where the cation is fully protected by the ligand from nonradiative deactivation, whereas the corresponding Yb^{3+} chelates have quantum yields only *ca.* five times lower in comparison to the nonhydrated analogues.[31,37,38] The Yb^{3+} quantum yields of these isoquinoline complexes are, however, higher than those measured for the versatile tropolonate ligand.[28] The best quantum yields are about two times higher than those of the parent pyridine complexes and are measured for the unsubstituted and the *p*-dimethoxyisoquinoline complexes. Further studies are in progress to better understand the energy transfer mechanism in those compounds on the basis of the electronic structure of the different lanthanide sensitizers.

In order to establish a proof of principle of the ability of these complexes to act as near-infrared emitting reporters in biological imaging, we have recorded images in capillaries filled with an Yb**L3** solution in fetal bovine serum (FBS) using a Nikon AZ-100 macroscope (Figure 6). The specific NIR emission arising from Yb^{3+} in Yb**L3** can be easily detected with the macroscope for a complex concentration of only 10 μM (Figure 6a). A comparison with the corresponding Eu**L3** complex demonstrates the advantages of NIR luminescence. When using visible detection, both the capillaries containing only FBS (blank) and those containing Eu**L3** in FBS are emissive, without any significant difference (Figure 6b). Upon NIR detection, the autofluorescence originating from FBS completely disappears and the luminescence of Yb**L3** in FBS can be unambiguously ascribed to the optical probe.

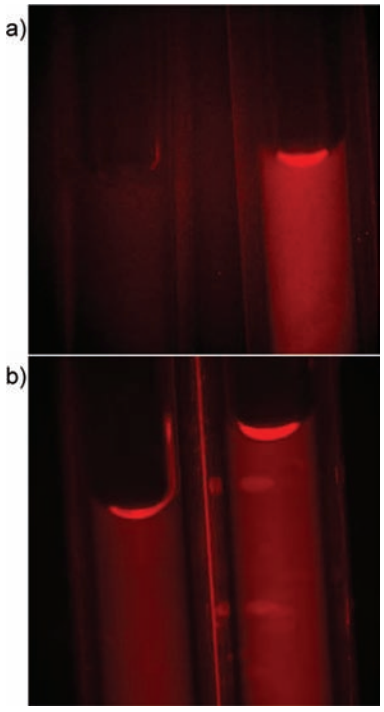

Figure 6. Optical images of (a) FBS (left) and 10 μM Yb**L3** in FBS (right), with λ_{em} = 975−1150 nm (selection with the help of a filter), and 60 s integration time ; (b) FBS (left) and 10 μM Eu**L3** (right) with a long-path emission filter with a 561 nm cutoff, and 100 ms integration time. The images are obtained with an excitation at 377 nm, and a 5-fold magnification.

3. CONCLUSION

Three isoquinoline-based poly(aminocarboxylate) ligands have been studied from the perspective of simultaneously ensuring

dx.doi.org/10.1021/ic202446e | *Inorg. Chem.* 2012, 51, 2522−2532

advantageous NIR optical and MR imaging properties when complexed to Yb^{3+}/Nd^{3+} and Gd^{3+}, respectively. A mixture of such complexes can therefore be applied for bimodal imaging applications providing identical biodistribution of the MRI and optical probes, thus straightforward merging of the MR and optical images. The lanthanide complexes formed with these isoquinoline-based ligands integrate several positive features. They are bishydrated and possess good thermodynamic stability and good selectivity for lanthanides versus endogenous cations. The Gd^{3+} complexes display faster water exchange than the clinically used MRI contrast agents, and the exchange proceeds via a dissociative mechanism as evidenced by the positive activation volumes.

In comparison to previously studied pyridine-based analogues, the isoquinoline core leads to an important decrease of the excitation energies of the NIR emitting lanthanide complexes, which therefore become more suitable for biological applications. The best ligand, **L3**, based on the *p*-dimethoxy-isoquinoline moiety, benefiting from the electron donating capacities of the methoxy groups, can be excited at a wavelength of 420 nm, more than 100 nm higher than the pyridine-based system. Our results evidence that such pyridine-based ligands can be easily modified to optimize the optical properties of the luminescent lanthanide complexes while retaining good stability and MRI properties for the Gd^{3+} complexes. The luminescence quantum yields of the Nd^{3+} and Yb^{3+} chelates are in the range of those for the best nonhydrated complexes, despite the presence of two inner sphere water molecules. As a consequence, we have been able to use these compounds in a proof of principle feasibility microscopy experiment where the signal of Yb^{3+} of one of these complexes could be easily monitored with a good signal-to-noise ratio. To the best of our knowledge, this is the first observation of a NIR signal arising from a Ln^{3+} complex in aqueous solution in a microscopy setup. Given the presence of two inner sphere water molecules, important for MRI applications of the corresponding Gd^{3+} analogues, this result is particularly exciting and opens wide perspectives not only for NIR imaging based on Ln^{3+} ions but also for the design of combined NIR optical and MRI probes.

4. EXPERIMENTAL SECTION

Materials and Methods. Lanthanide chloride ($GdCl_3$, $NdCl_3$, $EuCl_3$ and $LuCl_3$) or oxide (Yb_2O_3) salts were purchased from Aldrich. Solutions of Ln^{3+} and other cations (Ca^{2+}, Zn^{2+} and Cu^{2+}) were prepared in double distilled water, and their concentration was determined by complexometric titration with a standardized Na_2H_2EDTA solution using xylenol orange as indicator. The concentration of the ligand solutions was determined by adding an excess of Gd^{3+}, followed by complexometric titration of the noncomplexed Gd^{3+} with standardized Na_2H_2EDTA using xylenol orange as indicator in urotropine buffer (pH 5.6−5.8). The different complexes were prepared by mixing equimolar quantities of the cation and ligand solutions. The absence of free metal was checked with xylenol orange.

Synthesis of the Ligands. *(2E,3E)-3-Methyl-4-phenylbut-3-en-2-one Oxime (**1**).* This product is synthesized in two steps. Dry HCl was passed into a mixture of benzaldehyde (10.2 mL, 0.1 mol) and butanone (17.9 mL, 2 equiv) until the solution was saturated with gas. The mixture was stirred at room temperature for 8 h and evaporated. The crude oil was purified by flash chromatography on silica gel (dichloromethane/petroleum ether (7:3)) to give (*E*)-3-methyl-4-phenylbut-3-en-2-one (90%) as yellow oil.

Spectral and physical data were in accordance with the literature.[10]

A mixture of (*E*)-3-methyl-4-phenylbut-3-en-2-one (1 g, 6.24 mmol), hydroxylamine hydrochloride (0.65 g, 1.5 equiv) and pyridine (0.76 mL, 1.5 equiv) in EtOH (20 mL) was refluxed overnight. After being cooled to room temperature, the solvent was evaporated. The medium was dissolved in dichloromethane (20 mL), and water (10 mL) was added. The phases were separated, and the aqueous phase was extracted with dichloromethane (10 mL). Organic phases were brought together, dried over $MgSO_4$, and filtered, and the solvent was evaporated under reduced pressure. The crude oil was purified by flash chromatography on silica gel (dichloromethane/petroleum ether (7:3)) to give compound **1** (92%) as a yellow solid.

Spectral and physical data were in accordance with the literature.[10]

*1,3-Dimethylisoquinoline (**2**).* To a solution of PCl_5 (4.75 g, 1 equiv) in decalin (75 mL) was added a solution of oxime **1** (4 g, 22.8 mmol) in CH_2Cl_2 (10 mL) at 0 °C. The mixture was stirred at 0 °C for 10 min, and P_2O_5 (22 g, 1 g/mmol of oxime **1**) was added. The mixture was stirred at 180 °C for 30 min. After being cooled to 0 °C, the medium was hydrolyzed with water (20 mL) and a solution of NaOH 6 N (30 mL) until pH 12. The phases were separated, and the aqueous phase was extracted with ethyl acetate (3 × 30 mL). The combined organic phases were dried over $MgSO_4$ and filtered, and the solvent was evaporated under reduced pressure. The crude oil was purified by flash chromatography on silica gel (100% petroleum ether to remove decalin, then progressively 100% CH_2Cl_2 to eliminate impurities and finally progressively 100% ethyl acetate) to give compound **2** (60%) as a yellow oil.

Spectral and physical data were in accordance with the literature.[10]

*1,3-Bis(bromomethyl)isoquinoline (**3**).* A mixture of **2** (2.48 g, 15.8 mmol), NBS (16.9 g, 6 equiv) and dibenzoyl peroxide (0.1 g, 0.41 mmol) in CCl_4 (100 mL) was refluxed overnight. After cooling down to room temperature, the mixture was filtered, and the filtrate was successively washed with a saturated solution of sodium bicarbonate (30 mL) and a saturated solution of sodium thiosulfate (30 mL). The organic phase was dried over $MgSO_4$ and filtered, and the solvent was evaporated. To a solution of the crude product in THF (60 mL) were added diisopropylethylamine (6.7 mL, 4 equiv) and diethyl phosphite (5.2 mL, 4 equiv) at 0 °C. The mixture was stirred at room temperature for 5 h, poured in ice and extracted with ethyl acetate (40 mL). The organic phase was dried over $MgSO_4$ and filtered, and the solvent was evaporated under reduced pressure. The crude oil was purified by flash chromatography on silica gel (petroleum ether/ethyl acetate (1:1)) to afford compound **3** (35%) as a white solid.

Spectral and physical data were in accordance with the literature.[11]

*2,2′,2″,2‴-(Isoquinoline-1,3-diylbis(methylene))bis(azanetriyl)-tetraacetic Acid (**L1**).* To a solution of compound **3** (0.95 g, 3.02 mmol) in acetonitrile (40 mL) were successively added diethyl iminodiacetate (1.0 mL, 2 equiv), potassium carbonate (1.63 g, 4 equiv) and potassium iodide (1.0 g, 2 equiv). The mixture was refluxed for 14 h, and, after being cooled to room temperature, the crude product was filtered through a pad of Celite and the filtrate was evaporated. The crude tetraester was used without further purification in the next step.

To a solution of crude tetraester in a mixture of THF/H_2O (1/1, 40 mL) was added lithium hydroxide (0.9 g, 12 equiv), and the solution was stirred for 12 h at room temperature. The solvent was then evaporated under reduced pressure, and the crude product was purified on a Dowex 1 × 2 100(Cl) ion-exchange resin. The resin was activated with a solution of sodium hydroxide (1 M, 20 mL) until pH 14 and washed with water (30 mL) until pH 7. After the deposit of the crude compound, the impurities were washed with a mixture of H_2O/MeOH (1/1, 50 mL) before elution of the product with pure formic acid (70 mL). Evaporation afforded ligand **L1** (89%) as a white solid. Spectral and physical data were in accordance with the literature.[39]

Ligands **L2** and **L3** were prepared according to the procedure previously described.[12]

Potentiometric Studies. Carbonate-free 0.1 M KOH and 0.1 M HCl were prepared from Fisher Chemicals concentrates. Potentiometric titrations were performed in 0.1 M aqueous KCl under nitrogen atmosphere, and the temperature was controlled to ±0.1 °C with a circulating water bath. The p[H] (p[H] = −log[H^+], concentration in molarity) was measured in each titration with a combined pH glass electrode (Metrohm) filled with 3 M KCl, and the titrant addition was automated by use of a 702 SM Titrino (Metrohm) system. The electrode was calibrated in hydrogen ion concentration by titration of

dx.doi.org/10.1021/ic202446e | *Inorg. Chem.* 2012, 51, 2522−2532

HCl with KOH in 0.1 M electrolyte solution.[40] A plot of meter reading versus p[H] allows the determination of the electrode standard potential ($E°$) and the slope factor (f). Continuous potentiometric titrations with HCl and KOH 0.1 M were conducted on 5 mL of aqueous solutions containing the ligands (**L1** 1.12 mM, **L2** 2.99 mM, **L3** 2.95 mM) in KCl 0.1 M, with 2 min waiting time between 2 points. The titrations of the metal complexes were performed on 5 mL solutions of **L1** (1.12 mM), **L2** (2.99 mM) and **L3** (2.95 mM) containing 1 equiv of metal cation, with 2 min waiting time between 2 points. The same experiments were performed with 2 equiv of Zn^{2+} as well to check the absence of dinuclear complex formation.

Experimental data were refined using the computer program Hyperquad 2008.[41] All equilibrium constants are concentration quotients rather than activities and are defined as

$$\beta_{mlh} = \frac{[M_m L_l H_h]}{[M]^m [L]^l [H]^h}$$

The ionic product of water at 25 °C and 0.1 M ionic strength is pK_w = 13.77.[13] Fixed values were used for pK_w, ligand acidity constants and total concentrations of metal, ligand and acid. All values and errors (twice the standard deviation) reported are at least the average of three independent experiments.

Relaxivity Profiles. Proton NMRD profiles were recorded on a Stelar SMARtracer Fast Field Cycling NMR relaxometer (0.01−10 MHz) and a Bruker WP80 NMR electromagnet adapted to variable field measurements and controlled by a SMARtracer PC-NMR console. The temperature was monitored by a VTC91 temperature control unit and maintained by a gas flow. The temperature was determined by previous calibration with a Pt resistance temperature probe. The longitudinal relaxation rates ($1/T_1$) were determined in water. The least-squares fit of the ^{1}H NMRD data was performed by using MicroMath Scientist version 2.0 (Salt Lake City, UT, USA). The concentrations and pH of solutions were as follows: Gd**L1** (1.0 mM, pH 6.7), Gd**L2** (9.9 mM, pH 6.8), Gd**L3** (10.0 mM, pH 6.8) in 0.1 M HEPES buffer.

Variable Temperature ^{17}O NMR Measurements. The longitudinal ^{17}O relaxation rates ($1/T_2$) and the chemical shifts were measured in aqueous solutions of GdLi (i = 1−3) in the temperature range 280−350 K, on a Bruker Avance 500 (11.7 T, 67.8 MHz) spectrometer. The temperature was calculated according to previous calibration with ethylene glycol and methanol.[42] An acidified water solution ($HClO_4$, pH 4.0) was used as reference. Transverse relaxation times (T_2) were obtained by the Carr−Purcell−Meiboom−Gill spin−echo technique.[43] The technique of the ^{17}O NMR measurements on Gd^{3+} complexes has been described elsewhere.[44] The samples were sealed in glass spheres fitted into 10 mm NMR tubes to avoid susceptibility corrections of the chemical shifts.[45] To improve the sensitivity, ^{17}O-enriched water (10% $H_2{}^{17}O$, CortecNet) was added to the solutions to reach around 1% enrichment. The concentrations and pH of solutions were as follows (limited by solubility): Gd**L1** (8.14 mM, pH 6.9), Gd**L2** (21.8 mM, pH 6.2), Gd**L3** (17.0 mM, pH 6.1) in water. The ^{17}O NMR data have been treated according to the Solomon−Bloembergen−Morgan theory of paramagnetic relaxation,[6] (see the Supporting Information). The least-squares fit of the ^{17}O NMR data was performed using Micromath Scientist version 2.0 (Salt Lake City, UT, USA). The reported errors correspond to two times the standard deviation.

Variable Pressure ^{17}O NMR Measurements. The transverse ^{17}O relaxation rates ($1/T_2$) were measured in aqueous solutions of GdLi (i = 1−3) in the pressure range 1−200 MPa at 70 °C, on a Bruker Avance 400 spectrometer equipped with a homemade high pressure probe head. The temperature was controlled by circulating fluid from a temperature bath and was measured by means of a built-in Pt resistor. The pressure dependence of the transverse relaxation rate of acidified water, used as a reference, was described by assuming an activation volume of +0.97 cm^3 mol^{-1}.[46] The concentrations and pH of solutions were as follows: Gd**L1** (11.5 mM, pH 6.5), Gd**L2** (8.0 mM, pH 6.7) in water.

Photophysical Measurements. A solution of Ln**L1** (1 mM, pH 7.0) was prepared in 0.01 M HEPES buffer, and solutions of Ln**L2** and Ln**L3** (1 mM, pH 6.8) were prepared in 0.1 M HEPES buffer. UV−visible absorption spectra were recorded at 25 °C using a Perkin-Elmer Lambda 9 spectrophotometer. Emission and excitation spectra were measured using a modified Jobin-Yvon Horiba Fluorolog-322 spectrofluorimeter equipped with an Electro-Optical Systems, Inc. DSS-IGA02TL cooled to 77 K near-infrared detector. Singlet and triplet states were recorded on the Gd^{3+} complexes upon appropriate excitation wavelength at room temperature (fluorescence mode) and 77 K (phosphorescence mode with 0.1 ms delay) respectively. Luminescence quantum yields were collected with an integration sphere developed by Frédéric Gumy and Prof. Jean-Claude G. Bünzli (Laboratory of Lanthanide Supramolecular Chemistry, École Polytechnique Féderale de Lausanne (EPFL), BCH 1402, CH-1015 Lausanne, Switzerland) and manufactured by GMP SA (Renens Switzerland), using a quartz tube sample holder. Spectra were corrected for variations in excitation lamp output, spectral responses of the excitation and emission gratings, response of the detector, and the use of neutral density filters, when applicable. The calculated values were determined by integrating the emission profiles, averaged from three independent trials, and substitution into the ratio of emitted photons over absorbed photons. Lanthanide-centered luminescence lifetimes were measured at 298 K using a Quantel YG 980 (266 nm, fourth harmonic) as the excitation source. Emission was collected at a right angle to the excitation beam, and wavelengths were selected using an interferential filter (990 nm, BP20). The signal was monitored by a Hamamatsu H10330-45 near-infrared detector, and was collected on a 500 MHz band-pass digital oscilloscope (Tektronix TDS 724C). Experimental luminescence decay curves were treated with Origin 8.0 software using exponential fitting models. Three decay curves were collected on each sample, and reported lifetimes are an average of at least three successful independent measurements. Epifluorescence images of the compounds were obtained using a Nikon AZ100 macroscope equipped with a Photometrics Evolve 512 EMCDD camera. Excitation was performed via a 350−400 nm band-pass filter (FF01-377/50-25, Semrock), and the dichroic mirror had a cutoff wavelength of 705 nm (FF705-Di01-25×36, Semrock). The emission was recorded through a 975−1150 nm band-pass filter (1063BP175-25, Omega Filters). A few microliters of the complexes were deposited inside a glass capillary (CAP5, Nichiryo). Images were acquired using a ×5 objective with good transmission in the NIR (AZ-Plan Fluor 5×, Nikon).

■ ASSOCIATED CONTENT

Supporting Information

Potentiometric titration curves, NMRD and ^{17}O data, UV−vis, excitation, and emission spectra. Equations used for the analysis of the ^{17}O data and the NMRD profiles. This material is available free of charge via the Internet at http://pubs.acs.org.

■ AUTHOR INFORMATION

Corresponding Author

*E-mail: stephane.petoud@cnrs-orleans.fr (S.P.), eva.jakabtoth@cnrs-orleans.fr (E.T.), franck.suzenet@univ-orleans.fr (F.S.).

■ ACKNOWLEDGMENTS

The authors acknowledge Agnès Pallier for recording some of the potentiometric data. This work was financially supported by the Ministère de l'Enseignement Supérieur et de la Recherche (FC), the Institut National du Cancer, La Ligue contre le Cancer, France, and was carried out in the frame of the European COST Action D38. S.P. acknowledges support from the Institut National de la Santé et de la Recherche Médicale (INSERM).

REFERENCES

(1) Caravan, P.; Ellison, J. J.; McMurry, T. J.; Lauffer, R. B. *Chem. Rev.* **1999**, *99* (9), 2293−2352.
(2) Montgomery, C. P.; Murray, B. S.; New, E. J.; Pal, R.; Parker, D. *Acc. Chem. Res.* **2009**, *42* (7), 925−937.
(3) Bünzli, J.-C. G. *Chem. Rev.* **2010**, *110* (5), 2729−2755.
(4) Frullano, L.; Meade, T. J. *J. Biol. Inorg. Chem.* **2007**, *12* (7), 939−949.
(5) Mulder, W. J. M.; Strijkers, G. J.; Donega, C. D. M.; Storm, G.; Griffioen, A. W.; Nicolay, K. *Nanoparticles in Biomedical Imaging*; Springer: New York, 2007.
(6) Toth, E.; Helm, L.; Merbach, A. E. Relaxivity of Gadolinium(III) complexes: theory and mechanism. In *The chemistry of contrast agents in medical magnetic resonance imaging*; Merbach, A. E., Toth, E., Eds.; Wiley: Chichester, 2001.
(7) dos Santos, C. M. G.; Harte, A. J.; Quinn, S. J.; Gunnlaugsson, T. *Coord. Chem. Rev.* **2008**, *252* (23−24), 2512−2527.
(8) Pellegatti, L.; Zhang, J.; Drahos, B.; Villette, S.; Suzenet, F.; Guillaumet, G.; Petoud, S.; Toth, E. *Chem. Commun.* **2008**, *48*, 6591−6593.
(9) Bonnet, C. S.; Buron, F.; Caillé, F.; Shade, C. M.; Drahos, B.; Pellegatti, L.; Zhang, J.; Villette, S.; Helm, L.; Pichon, C.; Suzenet, F.; Petoud, S.; Toth, E. *Chem.—Eur. J.* **2011**, DOI: 10.1002/chem.201102310.
(10) Zielinski, W. *Synthesis* **1980**, *1980* (01), 70−72.
(11) Yin, X.-H.; Tan, M.-Y. *Synth. Commun.* **2003**, *33* (7), 1113−1119.
(12) Caillé, F.; Buron, F.; Tóth, É.; Suzenet, F. *Eur. J. Org. Chem.* **2011**, (11), 2120−2127.
(13) Smith, R. M.; Motekaitis, R. J.; Martell, A. E. *NIST Standard Reference Database*.
(14) Chatterton, N.; Gateau, C.; Mazzanti, M.; Pecaut, J.; Borel, A.; Helm, L.; Merbach, A. *Dalton Trans.* **2005**, *6*, 1129−1135.
(15) Palinkas, Z.; Roca-Sabio, A.; Mato-Iglesias, M.; Esteban-Gomez, D.; Platas-Iglesias, C.; de Blas, A.; Rodriguez-Blas, T.; Toth, E. *Inorg. Chem.* **2009**, *48* (18), 8878−8889.
(16) Cacheris, W. P.; Quay, S. C.; Rocklage, S. M. *Magn. Reson. Imaging* **1990**, *8* (4), 467−481.
(17) Sarka, L.; Burai, L.; Brucher, E. *Chem.—Eur. J.* **2000**, *6* (4), 719−724.
(18) Mieville, P.; Jaccard, H.; Reviriego, F.; Tripier, R.; Helm, L. *Dalton Trans.* **2011**, *40* (16), 4260−4267.
(19) Fries, P. H.; Belorizky, E. *J. Chem. Phys.* **2005**, *123*, 12.
(20) Powell, D. H.; NiDhubhghaill, O. M.; Pubanz, D.; Helm, L.; Lebedev, Y. S.; Schlaepfer, W.; Merbach, A. E. *J. Am. Chem. Soc.* **1996**, *118* (39), 9333−9346.
(21) Livramento, J. B.; Helm, L.; Sour, A.; O'Neil, C.; Merbach, A. E.; Toth, E. *Dalton Trans.* **2008**, *9*, 1195−1202.
(22) Livramento, J. B.; Sour, A.; Borel, A.; Merbach, A. E.; Toth, V. *Chem.—Eur. J.* **2006**, *12* (4), 989−1003.
(23) Cossy, C.; Helm, L.; Merbach, A. E. *Inorg. Chem.* **1989**, *28* (14), 2699−2703.
(24) Burai, U.; Toth, E.; Bazin, H.; Benmelouka, M.; Jaszberenyi, Z.; Helm, L.; Merbach, A. E. *Dalton Trans.* **2006**, *4*, 629−634.
(25) Thompson, M. K.; Botta, M.; Nicolle, G. M.; Helm, L.; Aime, S.; Merbach, A. E.; Raymond, K. N. *J. Am. Chem. Soc.* **2003**, *125*, 14274−14275.
(26) Toth, E.; Helm, L.; Merbach, A. E.; Hedinger, R.; Hegetschweiler, K.; Janossy, A. *Inorg. Chem.* **1998**, *37*, 4104−4113.
(27) Swaddle, T. W.; Mak, M. K. S. *Can. J. Chem.* **1983**, *61*, 473−480.
(28) Zhang, J.; Badger, P. D.; Geib, S. J.; Petoud, S. *Angew. Chem., Int. Ed.* **2005**, *44* (17), 2508−2512.
(29) Zhang, J.; Petoud, S. *Chem.—Eur. J.* **2008**, *14* (4), 1264−1272.
(30) Werts, M. H. V.; Verhoeven, J. W.; Hofstraat, J. W. *J. Chem. Soc., Perkin Trans.* **2000**, *3*, 433−439.
(31) Comby, S.; Imbert, D.; Vandevyver, C.; Bünzli, J.-C. G. *Chem.—Eur. J.* **2007**, *13* (3), 936−944.
(32) Tallec, G.; Imbert, D.; Fries, P. H.; Mazzanti, M. *Dalton Trans.* **2010**, *39* (40), 9490−9492.
(33) Beeby, A.; Burton-Pye, B. P.; Faulkner, S.; Motson, G. R.; Jeffery, J. C.; McCleverty, J. A.; Ward, M. D. *Dalton Trans.* **2002**, *9*, 1923−1928.
(34) Faulkner, S.; Beeby, A.; Carrie, M. C.; Dadabhoy, A.; Kenwright, A. M.; Sammes, P. G. *Inorg. Chem. Commun.* **2001**, *4* (4), 187−190.
(35) Beeby, A.; Clarkson, I. M.; Dickins, R. S.; Faulkner, S.; Parker, D.; Royle, L.; de Sousa, A. S.; Williams, J. A. G.; Woods, M. *J. Chem. Soc., Perkin Trans.* **1999**, *3*, 493−503.
(36) Tallec, G.; Fries, P. H.; Imbert, D.; Mazzanti, M. *Inorg. Chem.* **2011**, *50* (17), 7943−7945.
(37) Comby, S.; Imbert, D.; Chauvin, A.-S.; Bünzli, J.-C. G. *Inorg. Chem.* **2006**, *45* (2), 732−743.
(38) Nonat, A.; Imbert, D.; Pecaut, J.; Giraud, M.; Mazzanti, M. *Inorg. Chem.* **2009**, *48* (9), 4207−4218.
(39) Mukkala, V. M.; Sund, C.; Kwiatkowski, M.; Pasanen, P.; Hogberg, M.; Kankare, J.; Takalo, H. *Helv. Chim. Acta* **1992**, *75* (5), 1621−1632.
(40) Martell, A. E.; Motekaitis, R. J. *Determination and use of stability constants*; VCH: 1992.
(41) Gans, P.; Sabatini, A.; Vacca, A. *Talanta* **1996**, *43*, 1739−1753.
(42) Raiford, D. S.; Fisk, C. L.; Becker, E. D. *Anal. Chem.* **1979**, *51* (12), 2050−2051.
(43) Meiboom, S.; Gill, D. *Rev. Sci. Instrum.* **1958**, *29* (8), 688−691.
(44) Micskei, K.; Helm, L.; Brucher, E.; Merbach, A. E. *Inorg. Chem.* **1993**, *32* (18), 3844−3850.
(45) Hugi, A. D.; Helm, L.; Merbach, A. E. *Helv. Chim. Acta* **1985**, *68* (2), 508−521.
(46) Ducommun, Y.; Earl, W. L.; Merbach, A. E. *Inorg. Chem.* **1979**, *18* (10), 2754−2758.